ACS Catalysis

Research Article

pubs.acs.org/acscatalysis

Rh/ZrP_2O_7 as an Efficient Automotive Catalyst for NO_x Reduction under Slightly Lean Conditions

Yuki Nagao,*[,†,‡] Yunosuke Nakahara,[†] Takahiro Sato,[†] Hironori Iwakura,[†] Shoya Takeshita,[‡] Saki Minami,[‡] Hiroshi Yoshida,[‡,§] and Masato Machida*[,‡,§]

[†]Catalysts Strategic Division, Engineered Materials Sector, Mitsui Mining & Smelting Co., Ltd., 1013-1 Ageoshimo, Ageo, Saitama 362-0025, Japan

[‡]Department of Applied Chemistry and Biochemistry, Graduate School of Science and Technology, Kumamoto University 2-39-1 Kurokami, Chuo, Kumamoto 860-8555, Japan

[§]Unit of Elements Strategy Initiative for Catalysts & Batteries, Kyoto University, Kyoto Daigaku Katsura, Saikyo, Kyoto 615-8520, Japan

Supporting Information

ABSTRACT: The three-way catalyst performances of honeycomb-coated Rh catalysts were studied on several metal phosphate supports ($AlPO_4$, YPO_4, ZrP_2O_7, and $LaPO_4$) using various simulated exhausts with different air-to-fuel ratios (A/F). These supports significantly improved the NO_x purification ($deNO_x$) efficiency under slightly lean conditions ($14.6 < A/F \leq 15.3$) as compared with conventional Rh/ZrO_2 catalysts. The $deNO_x$ activity exhibited the following sequence of increasing the mean electronegativity of the supports: $ZrO_2 < YPO_4 < LaPO_4 < AlPO_4 < ZrP_2O_7$. Although both NO−CO and NO−C_3H_6 reactions contributed to the $deNO_x$ process, the latter reaction was more favored on Rh/ZrP_2O_7 than on Rh/ZrO_2. Partially oxidized C_3H_6 was adsorbed on Rh/ZrP_2O_7 in the form of reactive aldehyde species, in contrast to the less-reactive carboxylate species adsorbed on Rh/ZrO_2. Furthermore, Rh oxide was more easily reduced to the active metallic state on ZrP_2O_7 compared with Rh/ZrO_2 when the atmosphere was changed from lean ($A/F > 14.6$) to rich ($A/F < 14.6$). Metallic Rh formed on ZrP_2O_7 was only slowly oxidized on exposure to excess O_2, whereas Rh on ZrO_2 was readily oxidized to less-active Rh_2O_3. The high activity of Rh/ZrP_2O_7 toward C_3H_6 oxidation via aldehyde species as well as the resistance of metallic Rh against reoxidation are considered to be possible reasons for the enhanced $deNO_x$ performance of this catalyst in a slightly lean region.

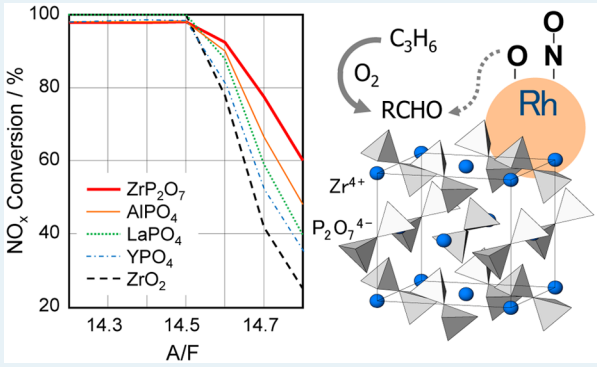

KEYWORDS: *three-way catalyst, rhodium, metal phosphate, lean NO_x reduction, honeycomb, air-to-fuel ratio*

INTRODUCTION

Currently, automotive three-way catalysts (TWCs) work efficiently to oxidize carbon monoxide (CO) and hydrocarbons (HC) and reduce nitrogen oxides (NO_x) simultaneously near the stoichiometric air/fuel (A/F) ratio of 14.6 on a weight basis, where NO_x reduction by CO and HC is possible. This state-of-the-art technology has been successfully utilized for gasoline-fueled vehicles since the 1970s and has largely contributed to global environmental protection.[1−5] Although engine control under fuel-lean conditions ($A/F > 14.6$) is better in terms of fuel efficiency, meaning that less CO_2 emissions are generated, NO_x reduction is not readily achieved in the presence of excess O_2. Rhodium (Rh) is the most important active component in TWCs, especially for converting NO_x into N_2,[6,7] but this reaction is strongly inhibited in excess O_2, which leads to the combustion of reducing gases (CO and HC) and the oxidation of metallic Rh to the less-active oxide (Rh_2O_3).[8] NO_x reduction under lean conditions—also called lean $deNO_x$—is thus a challenging issue that is still under investigation.

The physicochemical properties of Rh nanoparticles also depend on the support materials. Recently, we reported that $AlPO_4$ becomes a robust support material producing optimum interactions with the Rh species via Rh−O−P bonding, which can reduce the threshold loading owing to the high dispersion of oxidized Rh species anchored onto the phosphate unit on the surface.[9−11] The outstanding stability of $Rh/AlPO_4$ was demonstrated by thermal aging in a stream of air, where conventional Rh loaded on Al_2O_3 totally lost its catalytic activity as a result of solid-state reactions at the Rh_2O_3/Al_2O_3 interface. Because the interface Rh−O−P bonding forms in both an oxidizing and a reducing atmosphere, it affects the

Received: December 15, 2014
Revised: February 13, 2015
Published: February 13, 2015

DOI: 10.1021/cs5020157
ACS Catal. 2015, 5, 1986−1994

electronic states and redox behaviors of Rh. Actually, Rh_2O_3 is more reducible and the thus formed metallic Rh exhibits a higher tolerance against reoxidation when supported on $AlPO_4$ compared to Al_2O_3.[12] This unusual redox behavior of the Rh catalysts is expected to cause a positive impact on their lean $deNO_x$ performance.

In spite of such interesting characteristics, no other metal phosphates have been studied as support materials for Rh. In addition, the catalytic performances need to be evaluated in the form of honeycombs for practical applications in TWCs. In the present study, we have prepared monolithic honeycomb catalysts using four types of metal phosphates ($AlPO_4$, ZrP_2O_7, $LaPO_4$, and YPO_4) to study their TWC performance in simulated exhausts consisting of $NO-CO-C_3H_6-O_2-CO_2-H_2-H_2O$ mixtures as a function of A/F. Because the phosphate-supported catalysts showed higher lean $deNO_x$ efficiencies compared with conventional ZrO_2-supported Rh materials, we characterized them by Fourier transform infrared spectroscopy (FT-IR), X-ray absorption near edge structure (XANES), X-ray photoelectron spectroscopy (XPS), and temperature-programmed reduction/oxidation (TPR/TPO) to elucidate the reason for their improved catalytic performance, especially focusing on Rh/ZrP_2O_7, which exhibited the highest lean $deNO_x$ performance among all the studied materials.

EXPERIMENTAL SECTION

Catalyst Preparation. Four types of metal phosphates, namely, $AlPO_4$, YPO_4, ZrP_2O_7, and $LaPO_4$, were prepared by the coprecipitation method. Aqueous ammonia (5 mol L^{-1}) was added dropwise to an aqueous solution containing nitrate [$Y(NO_3)_3$, $ZrO(NO_3)_2$ or $La(NO_3)_3$] and H_3PO_4 (Wako Pure Chemical Industries, Ltd.) with stoichiometric molar ratio under vigorous stirring until the pH reached 9.0. The precipitate thus formed was washed with deionized water, dried in air, and calcined at 900 °C for 5 h in air. $AlPO_4$ was also prepared in a similar way, but the precipitate formed until the pH had reached 4.5 was washed with deionized water, dried in air, and calcined at 1000 °C for 5 h in air.[9,11] A reference support, ZrO_2, was supplied by the Catalysis Society of Japan (JRC-ZRO-3) and calcined at 600 °C before use.

Supported Rh catalysts with different loadings (i.e., 0.15 and 0.5 wt % as Rh metal) were prepared by impregnation of an aqueous solution of $Rh(NO_3)_3$ (Tanaka Noble Metals Co, Ltd.), followed by drying and calcination at 600 °C for 3 h in air. 0.5 wt % Rh loaded powders were used for the catalytic activity test and characterization. Monolithic honeycomb catalysts were prepared by dipping a cordierite honeycomb (25.4 mmφ × 30 mm, 600 cells in^{-2}, NGK Insulators, Ltd.) into a slurry, which was prepared by ball-milling of the catalyst powders (0.15 wt % Rh), an inorganic binder, and water, followed by drying at 90 °C for 15 min and calcination in air at 600 °C for 3 h. The as-calcined honeycomb catalysts contained about 100 g L^{-1} of coated catalyst powders so that the total Rh loading was 0.15 g L^{-1}. Prior to the catalytic tests, the honeycomb catalysts were thermally aged at 800 °C for 50 h by switching two gas streams between reducing (A/F = 13.0, 90 s) and oxidizing (air, 10 s) conditions.

Catalyst Characterization. X-ray diffraction (XRD) patterns of the catalyst powders were recorded using a Rigaku RINT-TTRIII diffractometer with Cu Kα radiation (50 kV, 30 mA). The microstructure of the honeycomb catalysts was observed using a scanning electron microscope (Hitachi Miniscope TM3000). The Brunauer−Emmett−Teller (BET) surface area (S_{BET}) was calculated from N_2 adsorption isotherms (Quantachrome Instrument, Quadrasorb SI) measured at 77 K. Rh metal dispersion was measured by the CO chemisorption method.[13] Prior to the measurements, the catalyst powders (0.2 g) were treated at 400 °C in flowing air, followed by reduction in the presence of H_2. After the samples were cooled to 50 °C, CO pulse injection was performed in an He stream. Metal dispersion was evaluated in terms of CO/Rh, which is the molar ratio between chemisorbed CO and loaded Rh.

In situ XANES measurements on Rh at the K-edge were performed at the BL14B2 beamline of SPring-8 with the approval of the Japan Synchrotron Radiation Research Institute (Proposal No. 2013A1344). An Si(111) crystal monochromator was used. The catalyst powders were pressed into a disc of about 1 g and placed in a quartz *in situ* cell. The measurements were conducted at 500 °C in streams of gas mixtures consisting of 20% O_2 balanced with He or 0.5% CO and 0.2% NO balanced with He (A/F = 14.0). The obtained data were processed using the Athena program.[14] The oxidation state of Rh was determined using Rh_2O_3 and an Rh foil as a reference. XPS studies were performed on a Shimadzu-Kratos AXIS Ultra spectrometer equipped with a monochromatic Al Kα X-ray source (15 kV, 10 mA) and a delay-line detector. The peak position was calibrated using the binding energy of C 1s (284.6 eV).

In situ FT-IR experiments were conducted on a Thermo 6700 spectrometer using a temperature-controllable diffuse reflectance reaction cell with a KBr window that was connected to a gas supply system to allow measurements in controlled gas environments at atmospheric pressure. The catalyst was placed in a crucible inside the cell and was then exposed to a flowing gas mixture. The sample was heated *in situ* under He flow at 500 °C for 30 min, followed by cooling to 300 °C and reduction by 5% H_2/He prior to all the experiments. Adsorption was induced at 300 °C by supplying gas mixtures containing 0.8% C_3H_6, 0.5% O_2, and He balance for 30 min, and subsequently 2.5% O_2/He or 1% NO/He. The spectrum was recorded in an He stream at the same temperature.

The temperature-programmed reduction by H_2 and reoxidation by O_2 (H_2-TPR/O_2-TPO) of the supported Rh materials were measured in a flow system. Prior to the measurements, the as-prepared powder catalysts were treated in a 20% O_2 flow balanced with He at 400 °C for 30 min. After cooling, the catalysts were heated up to 700 °C in a 5% H_2 flow balanced with He at a constant rate of 10 °C min^{-1}. After cooling down to ambient temperature, the catalysts were reheated in a 2.5% O_2 flow balanced with He at a constant rate of 10 °C min^{-1}. The concentrations of H_2 and O_2 in the effluent gas were analyzed by online quadrupole mass spectroscopy (Pfeiffer, Omnistar).

Catalytic Activity Tests. Catalytic activity tests on the powder catalysts (0.5 wt % Rh) were performed in a flow reactor at atmospheric pressure. The catalyst powder (100 mg) was fixed in a quartz tube using quartz wool at both ends of the catalyst bed. The catalyst bed was then heated from 120 to 700 °C at a constant rate of 10 °C·min^{-1} while supplying a simulated exhaust gas mixture containing CO (0.5%), H_2 (0.17%), C_3H_6 (400 ppm), NO (500 ppm), O_2 (0.50%), CO_2 (14.0%), H_2O (10.0%), and N_2 balance at 1 L·min^{-1} (W/F = 0.1 g·min·L^{-1}). The gas composition corresponds to the stoichiometric air-to-fuel ratio A/F = 14.6. The A/F value is

DOI: 10.1021/cs5020157
ACS Catal. 2015, 5, 1986−1994

calculated according to the literature[15] using following excess oxygen ratio of the simulated gas feed.

$$\text{Excess oxygen ratio} = \frac{\text{Amount of oxygen in gas feed}}{\text{Amount of oxygen required for complete oxidation}} = \frac{2 \times p_{O_2} + p_{NO}}{9 \times p_{C_3H_6} + p_{CO} + p_{H_2}}$$

Catalytic activity tests on the honeycomb catalysts were performed in a flow reactor in four different modes (A, B, C, and D) at atmospheric pressure. Modes A and B used gas mixtures containing CO, C_3H_6, H_2, NO, O_2, CO_2, H_2O, and N_2 balance (with varying A/F values), whereas modes C and D used similar gas mixtures but excluding C_3H_6 and CO, respectively (see Supporting Information for detailed gas compositions of the different A/Fs in each mode). The honeycomb catalysts were fixed in a tubular reactor, and their catalytic activity was evaluated as a function of A/F by supplying simulated gas mixtures preheated at 400 °C to the tubular reactor at a space velocity of SV = 98 000 h^{-1}. The catalytic light-off of a stream of C_3H_6 (550 ppm), O_2 (0.3%), H_2O (10%), and N_2 balance (A/F = 14.7) was also measured at a heating rate of 10 °C min^{-1} to analyze the products of C_3H_6 oxidation. The concentrations of CO, C_3H_6, and NO_x in the effluent gas were analyzed online using an exhaust gas analyzer (Best Sokki, SESAM3-N, and Bex-5200C) equipped with an FT-IR spectrometer and a flame ionization detector.

RESULTS AND DISCUSSION

Catalytic Performance of the Honeycomb Catalysts. Powders of the four metal phosphates ($AlPO_4$, YPO_4, ZrP_2O_7, and $LaPO_4$) were obtained as single phases (Supporting Information, Figure S1). Table 1 shows the surface area (S_{BET}), Rh metal dispersion (CO/Rh), and catalytic activity of the as-prepared powder catalysts. Although the S_{BET} of Rh-loaded catalyst was strongly dependent on the type of phosphates, the CO/Rh value was in the range of 20%−40% in all cases. The catalytic activity was measured in a light-off mode (10 °C·min^{-1}) and the conversion over the powder catalysts increased very steeply to 100% within a narrow temperature range. Because it is difficult to compare the reaction rate under kinetically limited conditions at the same temperature, the activity here is simply expressed in terms of the light-off temperature (T_{50}) at which the conversion of CO, C_3H_6, and NO_x reached 50%. The studied catalysts showed no significant difference in this value at stoichiometric gas mixtures (A/F = 14.6).

Table 1. Specific Surface Area, Rh Metal Dispersion, and Catalytic Activity of As-Prepared Powder Catalysts (0.5 wt % Rh loading)

sample	S_{BET}[a] / $m^2 \cdot g^{-1}$	CO/Rh[b] (%)	T_{50}/°C[c] CO	C_3H_6	NO_x
$Rh/AlPO_4$	74	37	233	264	235
Rh/YPO_4	49	33	239	287	247
Rh/ZrP_2O_7	7	22	231	283	252
$Rh/LaPO_4$	37	27	234	268	239
Rh/ZrO_2	61	38	227	286	258

[a]BET surface area of Rh-loaded catalysts. [b]Molar ratio of CO chemisorbed to Rh loaded. [c]Temperature at which CO, C_3H_6, and NO_x conversions reached 50%. CO (0.5%), H_2 (0.17%), C_3H_6 (400 ppm), NO (500 ppm), O_2 (0.50%), CO_2 (14.0%), H_2O (10.0%), N_2 balance, W/F = 0.1 g·min·L^{-1}, A/F = 14.6.

Figure 1 shows a scanning electron microscopy (SEM) image of the fracture surface of an as-prepared honeycomb catalyst

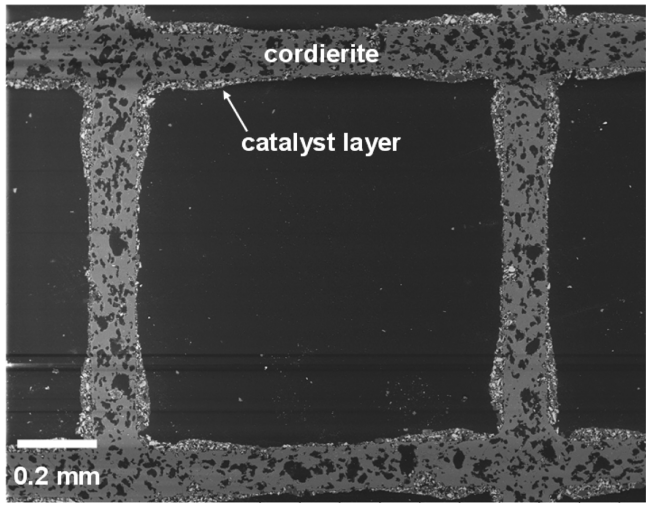

Figure 1. SEM image of Rh/ZrP_2O_7-coated monolithic honeycomb catalyst.

with a washcoat layer (20 μm thick) consisting of Rh/ZrP_2O_7. This layer is in intimate contact with the surface of the cordierite honeycomb substrate. Similar microstructures were observed for other honeycomb catalysts consisting of Rh supported on metal phosphates and ZrO_2. The catalytic activity of the honeycomb catalysts was evaluated in a steady-state mode using four different simulated exhaust gas mixtures (designated as modes A, B, C, and D). Figure 2 compares the conversions of CO, C_3H_6, and NO_x at 400 °C for the studied honeycomb catalysts in the range of $14.2 \leq A/F \leq 14.8$ (mode A). CO and C_3H_6 conversions occurred to more than 80% in the lean region (A/F > 14.6), where complete oxidation is preferred in excess O_2. On the other hand, conversions in the rich region (A/F < 14.6) are influenced by steam-reforming (C_3H_6−H_2O) and water−gas shift (CO−H_2O) reactions, which occur preferentially on Rh/ZrO_2 rather than on Rh catalysts supported on metal phosphates.[12] Although NO_x conversion was nearly complete in the rich region (A/F < 14.6), it decreased in the lean region (A/F > 14.6), where excess oxygen inhibited NO_x reduction. Note that NO_x conversion at A/F > 14.6 is strongly dependent on the support materials and that the following sequence is obtained: ZrP_2O_7 > $AlPO_4$ > $LaPO_4$ > YPO_4 > ZrO_2.

Because Rh/ZrP_2O_7 showed the highest lean deNO_x performance, the following studies were focused on this catalyst compared with Rh/ZrO_2, which was used as a reference catalyst. Figure 3 compares the conversions over Rh/ZrP_2O_7 and Rh/ZrO_2 in the broad lean region ($14.6 \leq A/F \leq 15.3$, mode B) measured at 400 °C. Both catalysts exhibited NO_x conversion that decreased monotonically with increasing A/F values, but the negative slope of the curves near A/F = 14.7 was much more moderate for Rh/ZrP_2O_7, which means that this catalyst could preserve a higher NO_x conversion activity within a wide range of the lean region. NO_x reduction in the lean region was further studied using simple model systems with single reducing gases, i.e., either CO (mode C) or C_3H_6 (mode D), at 400 °C to identify which of the reducing

DOI: 10.1021/cs5020157
ACS Catal. 2015, 5, 1986−1994

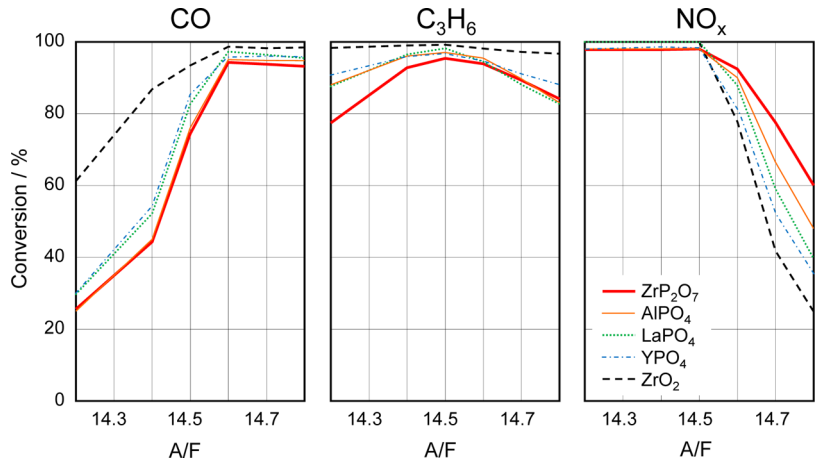

Figure 2. Catalytic conversion of CO, C_3H_6, and NO_x over honeycomb-supported Rh catalysts at 400 °C in the range of $14.2 \leq A/F \leq 14.8$ (mode A). CO (0.4−1.0%), H_2 (0.13−0.33%), C_3H_6 (400 ppm), NO (500 ppm), O_2 (0.6−0.35%), CO_2 (14.0%), H_2O (10.0%), N_2 balance, SV = 98 000 h^{-1}.

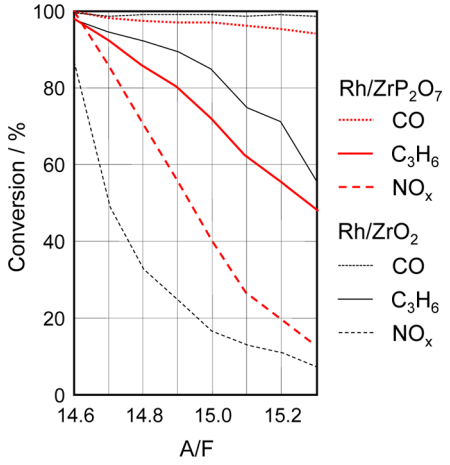

Figure 3. Catalytic conversion of CO, C_3H_6, and NO_x over Rh/ZrP_2O_7 and Rh/ZrO_2 honeycomb catalysts at 400 °C under lean conditions in the range of $14.6 \leq A/F \leq 15.3$ (mode B). CO (0.3−0.69%), C_3H_6 (400 ppm), NO (500 ppm), O_2 (0.93−0.50%), CO_2 (14.0%), H_2O (10.0%), N_2 balance, SV = 98 000 h^{-1}.

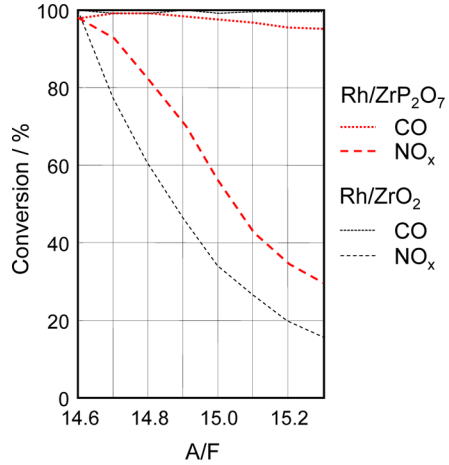

Figure 4. Catalytic conversion of CO and NO_x over Rh/ZrP_2O_7 and Rh/ZrO_2 honeycomb catalysts at 400 °C under lean conditions in the range of $14.6 \leq A/F \leq 15.3$ (mode C). CO (0.3−0.69%), NO (500 ppm), O_2 (0.41−0.32%), CO_2 (14.0%), H_2O (10.0%), N_2 balance, SV = 98 000 h^{-1}.

gases play a key role. In mode C (Figure 4), Rh/ZrP_2O_7 showed a higher NO_x conversion activity compared with Rh/ZrO_2, but the activity differences between the two catalysts were smaller than those observed in mode B (Figure 3). CO conversions in this region were more than 95% for both catalysts, suggesting that a large part of CO reacted with O_2. $DeNO_x$ activity differences were also observed in mode D (Figure 5). Rh/ZrO_2 exhibited NO_x conversions of ∼80% near the stoichiometric ratio (A/F = 14.6), whereas the values decreased steeply with increasing A/F. NO_x conversions over Rh/ZrP_2O_7 also showed a similar behavior but the obtained values were higher than those observed for Rh/ZrO_2. The activity differences were most significant at $A/F \approx 14.8$, where the NO_x conversion yield was 85% over Rh/ZrP_2O_7, compared to 25% over Rh/ZrO_2. Differences were also observed for C_3H_6 conversion. On Rh/ZrO_2, C_3H_6 conversion yields of 70%−80% were obtained in this region, whereas Rh/ZrP_2O_7 showed a higher C_3H_6 conversion activity that gradually decreased with increasing A/F. Because the C_3H_6 concentration in the gas feed was kept constant, the rate of C_3H_6 oxidation shows the negative dependence on the O_2 concentration. However, this is

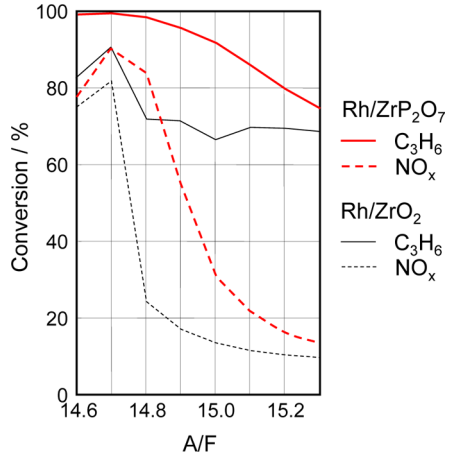

Figure 5. Catalytic conversion of C_3H_6 and NO_x over Rh/ZrP_2O_7 and Rh/ZrO_2 honeycomb catalysts at 400 °C under lean conditions in the range of $14.6 \leq A/F \leq 15.3$ (mode D). C_3H_6 (400 ppm), NO (500 ppm), O_2 (0.50−0.19%), CO_2 (14.0%), H_2O (10.0%), N_2 balance, SV = 98 000 h^{-1}.

DOI: 10.1021/cs5020157
ACS Catal. 2015, 5, 1986−1994

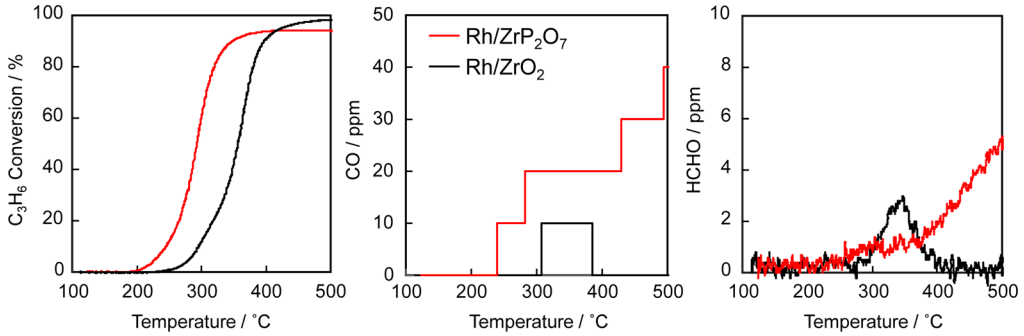

Figure 6. Catalytic conversion of C_3H_6 over Rh/ZrP_2O_7 and Rh/ZrO_2 honeycomb catalysts and CO and HCHO concentrations in the effluent gas for the $C_3H_6-O_2-H_2O$ reaction under a lean condition (A/F = 14.7). C_3H_6 (550 ppm), O_2 (0.3%), H_2O (10%), and N_2 balance, SV = 98 000 h^{-1}, 10 °C min^{-1}.

not consistent with the reported kinetic analysis of C_3H_6 oxidation over Rh catalysts under lean conditions, which shows a positive reaction order with respect to O_2.[16] The negative dependence of the present case can therefore be interpreted by inhibition of C_3H_6 oxidation due to the oxidation of Rh. It should be noted that Rh/ZrO_2 exhibited a steep drop of C_3H_6 conversion at A/F = 14.8, which should be associated with faster oxidation of Rh compared to Rh/ZrP_2O_7 as discussed later.

The results shown in Figures 4 and 5 suggest that the NO–C_3H_6 reaction contributes more significantly than the NO–CO reaction to the lean deNO_x process over Rh/ZrP_2O_7. The C_3H_6 oxidation behavior of the two honeycomb catalysts in a slightly lean region was further studied focusing on the reaction products. An infrared gas analysis was conducted to detect CO and HCHO during C_3H_6 oxidation. The concentrations of these two compounds in the effluent gas are plotted in Figure 6 when mixtures of $C_3H_6-O_2-H_2O$ (A/F = 14.7) were supplied as the gas feed. Rh/ZrP_2O_7 caused a light-off of the stream at around 200 °C, compared to the 250 °C required for Rh/ZrO_2. Nevertheless, the conversion over Rh/ZrP_2O_7 leveled off above 400 °C, where the concentrations of CO and HCHO increased with an increase in the reaction temperature. This is in complete contrast to what was observed on Rh/ZrO_2, where only the temporary formation of these partially oxidized products occurred. These results clearly suggest that the Rh/ZrP_2O_7 catalyst exhibits a higher C_3H_6 oxidation activity and a higher selectivity to partially oxidized products under lean conditions. As shown in Table 1, Rh/ZrP_2O_7 exhibited the lowest surface area and Rh metal dispersion, which cannot rationalize the high catalytic activities for lean deNO_x and C_3H_6 oxidation. It is therefore suspected that intermediate species during C_3H_6 oxidation over the catalyst play a key role in these reactions.

Adsorbed Species of Partially Oxidized C_3H_6. To elucidate the reasons for the high lean deNO_x efficiency of the studied materials, *in situ* FT-IR spectra of the powdered catalysts were recorded during the $C_3H_6-O_2$ reaction. Figure 7 shows the spectra of the adsorbed species for Rh catalysts supported on metal phosphates and ZrO_2. All the spectra were measured at 300 °C and referenced to the spectrum of a sample in a He flow just before exposure to C_3H_6/O_2. The assignment of absorption bands described below is consistent with those previously reported by several researchers.[17−19] Rh/ZrO_2 showed strong bands due to carboxylate COO^- (1440 and 1560 cm^{-1}), formate $HCOO^-$ (1365 and 1610 cm^{-1}), and dicarbonyl $(CO)_2$ (1990 and 2070 cm^{-1}). Unlike Rh/ZrO_2, the

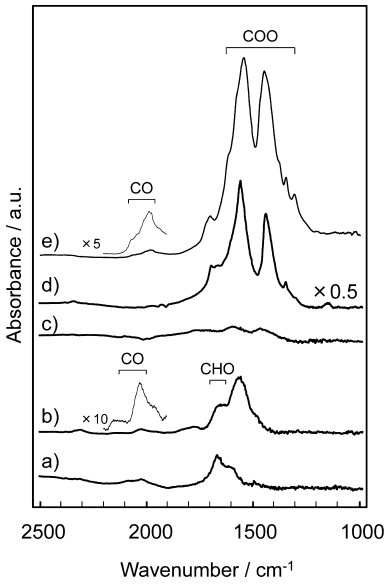

Figure 7. *In situ* diffuse reflectance FT-IR spectra of adsorbed species formed on powder catalysts in gas mixtures containing 0.8% C_3H_6, 0.5% O_2, and He balance at 300 °C: (a) $Rh/AlPO_4$, (b) Rh/ZrP_2O_7, (c) Rh/YPO_4, (d) $Rh/LaPO_4$, and (e) Rh/ZrO_2 at 300 °C.

Rh catalyst supported on ZrP_2O_7 and $AlPO_4$ yielded less intense bands in this region, which were assignable to allylaldehyde–CHO (1670 cm^{-1}) and dicarbonyl $(CO)_2$ (2030 and 2110 cm^{-1}). Although dicarbonyl species should be adsorbed on Rh, the phosphate supports lead to a shift of the bands to higher wavenumbers because their electron-drawing effect generates electron-deficient Rh species, thus retarding back-donation from the Rh *d*-orbitals to the antibonding π^* orbitals of CO.[12] On the other hand, carboxylate and aldehyde are considered to form and adsorb on the surface of the supports because bands with almost the same intensity could be observed for Rh-free samples (see Supporting Information). The amount of partially oxidized species adsorbed on the phosphate surface was approximately 1 × 10^{-4} mol-C·g^{-1}. Similarly, carboxylate species were formed on the surface of ZrO_2. Furthermore, aldehyde/carboxylate bands with similar intensities were observed not only under rich (O_2/C_3H_6 < 4.5) but also under lean (O_2/C_3H_6 > 4.5) conditions (see Supporting Information). Rh catalysts loaded on other phosphates, such as YPO_4 and $LaPO_4$, showed intermediate behaviors, forming both carboxylate and aldehyde.

DOI: 10.1021/cs5020157
ACS Catal. 2015, 5, 1986−1994

This is reasonable considering the lower acidity of YPO_4 and $LaPO_4$ compared to ZrP_2O_7 and $AlPO_4$, as discussed later.

It is known from the literature that the oxidation of C_3H_6 proceeds via π-allyl complexes,[20] which may undergo an abstraction of α-hydrogen followed by the insertion of oxygen to an allylic C−H bond.[21] In general, chemisorption of C_3H_6 occurs on the Lewis acid site and the abstraction of α-hydrogen is accomplished on the Brønsted sites.[22] Because the surface of ZrP_2O_7 and $AlPO_4$ are terminated by P−OH and Al−OH/Zr−OH groups,[12] these moieties possibly act as acid sites. FT-IR measurement of pyridine chemisorption demonstrated that ZrP_2O_7 contained both Brønsted and Lewis acid sites, whereas ZrO_2 had only Lewis acidity (see Supporting Information). $AlPO_4$ also shows Brønsted and Lewis acidity,[12] but other phosphates (YPO_4 and $LaPO_4$) showed very weak acidity. The difference of adsorbed C_3H_6 species between ZrP_2O_7 and ZrO_2 is therefore possibly associated with the nature of their acid sites.

Next, the reactivity of the partially oxidized C_3H_6 species adsorbed on ZrP_2O_7 and ZrO_2 was studied (Figure 8). After

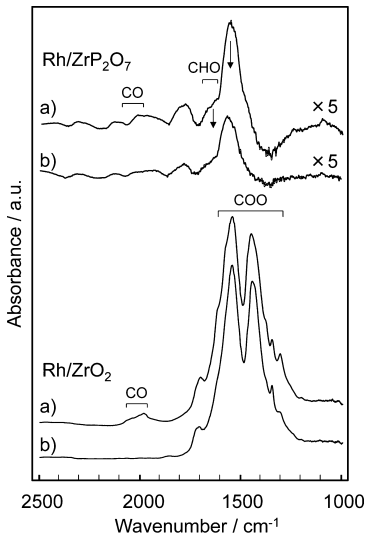

Figure 8. *In situ* diffuse reflectance FT-IR spectra of adsorbed species formed on Rh/ZrP_2O_7 and Rh/ZrO_2: (a) in gas mixtures containing 0.8% C_3H_6, 0.5% O_2, and He balance at 300 °C and (b) subsequent admission of 2.5% O_2/He for 10 min.

exposure to 2.5% O_2/He at 300 °C for 10 min, the aldehyde (1670 cm^{-1}) and CO (2030 and 2100 cm^{-1}) bands on Rh/ZrP_2O_7 were less intense as shown by arrows, and the simultaneous formation of CO_2 was detected by a parallel evolved gas analysis performed using online mass spectroscopy. This result is indicative of the spillover of oxygen, followed by reaction with aldehyde species on ZrP_2O_7. However, this is not the case for Rh/ZrO_2, where the carboxylates remained unchanged, probably because of its lower reactivity compared to the aldehyde species on Rh/ZrP_2O_7. The reactivity of these partially oxidized C_3H_6 species to NO was also studied (Figure 9). When 1% NO/He was supplied to Rh/ZrP_2O_7 at 300 °C for 10 min, a band corresponding to NO adsorbed on Rh (1920 cm^{-1}) appeared, with a simultaneous decrease in the aldehyde band. This is different from the results obtained for Rh/ZrO_2, where only a negligible change in the carboxylate bands was observed. Considering that aldehyde-type adsorbates can be formed on ZrP_2O_7, even in the presence of excess O_2, these

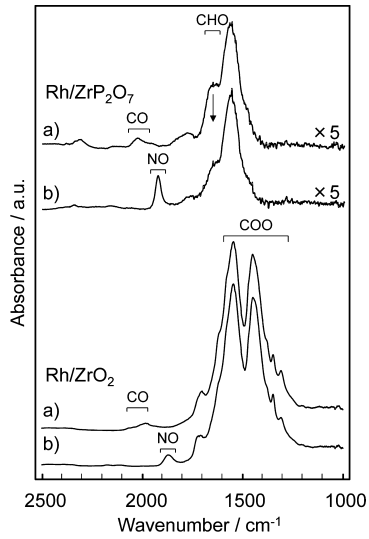

Figure 9. *In situ* diffuse reflectance FT-IR spectra of adsorbed species formed on Rh/ZrP_2O_7 and Rh/ZrO_2: (a) in gas mixtures containing 0.8% C_3H_6, 0.5% O_2, and He balance at 300 °C and (b) subsequent admission of 1% NO/He for 10 min.

species should play a role as reducing agents in the lean deNO_x process. ZrP_2O_7 is apparently able to store these reducing agents on its surface and supply them to the Rh/ZrP_2O_7 perimeter, where the reaction with adsorbed O_2 and NO species may be possible. In contrast, the carboxylate species formed on Rh/ZrO_2 are too stable to contribute to the reaction with O_2 and/or NO. In both cases, partial oxidation of C_3H_6 yielded CO adsorbed on Rh, which was immediately consumed by the reaction with O_2 and NO (Figures 8 and 9).

Oxidation State of Rh. Because Rh oxide (Rh_2O_3) is thermodynamically stable in O_2 up to approximately 900 °C, the extent of oxidation affects the catalytic activity in the lean region. The oxidation state of Rh under lean and rich conditions was thus studied by *in situ* XANES. Figure 10 shows the XANES spectra of Rh/ZrP_2O_7 and Rh/ZrO_2 powders. The fractions of metallic Rh (Rh^0) and oxidized Rh (Rh^{3+}) were estimated by curve-fitting analysis using two references (a Rh foil and Rh_2O_3). When Rh/ZrO_2 was treated

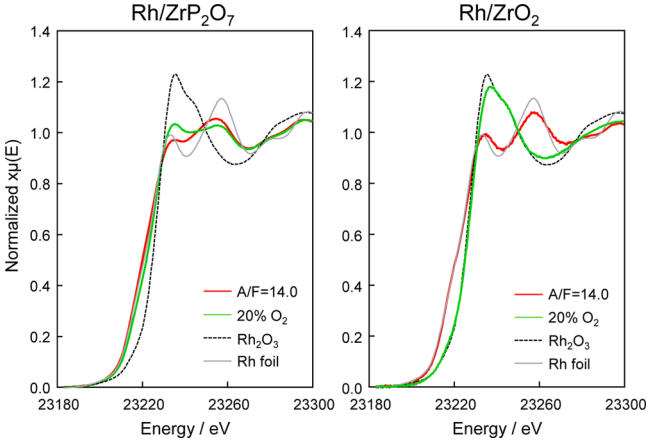

Figure 10. *In situ* XANES spectra of Rh/ZrP_2O_7 and Rh/ZrO_2 after treatment in a reducing atmosphere (A/F = 14.0) and subsequently in an oxidizing atmosphere (20% O_2) at 500 °C. An Rh foil and Rh_2O_3 are shown as references.

DOI: 10.1021/cs5020157
ACS Catal. 2015, 5, 1986−1994

in gas mixtures containing 0.5% CO and 0.2% NO balanced with He (corresponding to rich conditions, A/F = 14.0) at 500 °C for 60 min, the spectrum was quite similar to that of metallic Rh (96% Rh^0). However, upon switching the gas feed to 20% O_2/He for 40 min, the spectrum changed to show a nearly stoichiometric oxidation to Rh_2O_3 (13% Rh^0). The reduction/reoxidation of Rh was thus almost reversible on ZrO_2. However, this was not the case for Rh/ZrP_2O_7; Rh was close to the metallic state (81% Rh^0) under rich conditions (A/F = 14.0) and remained almost unchanged (70% Rh^0), even after switching to 20% O_2/He. The metallic Rh species on ZrP_2O_7 should therefore be substantially stabilized against reoxidation.

Figure 11 shows the Rh 3d XPS spectra of Rh/ZrP_2O_7 and Rh/ZrO_2 powders before and after exposure to rich gas

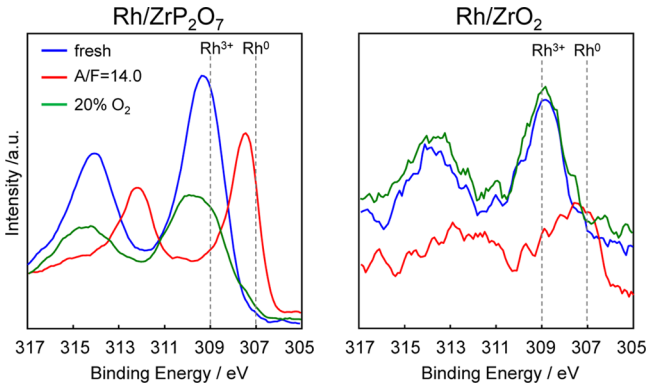

Figure 11. Rh 3d XPS spectra of Rh/ZrP_2O_7 and Rh/ZrO_2 before and after treatment in a reducing atmosphere (A/F = 14.0) and subsequently in an oxidizing atmosphere (20% O_2) at 500 °C. Dashed lines show the literature Rh $3d_{5/2}$ data for Rh metal (Rh^0) and Rh_2O_3 (Rh^{3+}).[23,48]

mixtures with A/F = 14.0 at 500 °C, and subsequently to 20% O_2/He. Both catalysts (calcined at 600 °C) exhibited a binding energy of approximately 309 eV (Rh $3d_{5/2}$), which is higher than the value obtained for Rh^0 (~307 eV), indicating that the surface of Rh is oxidized (Rh^{3+}). Large parts of the Rh surface of both catalysts turned into the metallic state upon exposure to a reducing gas mixture with A/F = 14.0, where the fraction of Rh^0 was 62% for Rh/ZrO_2, compared to 65% for Rh/ZrP_2O_7. Here, the Rh^0 peaks for Rh/ZrP_2O_7 showed shifts to higher binding energies (Rh $3d_{5/2}$: 307.5 eV) compared with those for the reported value[23] (Rh $3d_{5/2}$: 307.0 eV). This can be explained by the electron-deficient character of Rh that results from the electron-drawing effect of the acidic phosphate units.[11,12] Subsequent treatment in 20% O_2/He restored the oxidized Rh, but reversible reoxidation was only observed on Rh/ZrO_2, in contrast to the irreversible reoxidation behavior of Rh/ZrP_2O_7. XANES and XPS studies demonstrated the stability of metallic Rh against reoxidation on Rh/ZrP_2O_7. However, note that this trend is more obvious in Figure 10 than in Figure 11, possibly because the XANES results reflect the bulk information, whereas the XPS measurements are sensitive to the surface. The disagreement between the Rh oxidation states determined by XANES and XPS suggests the formation of egg-shell-like Rh_2O_3/Rh particles with a partially oxidized surface.

Because the XANES and XPS results suggested different reduction/reoxidation behaviors of the Rh catalysts depending on the support materials, H_2-TPR and O_2-TPO experiments were also performed (Figure 12). H_2 consumption due to the reduction of Rh oxide to metallic Rh yielded a peak at a lower

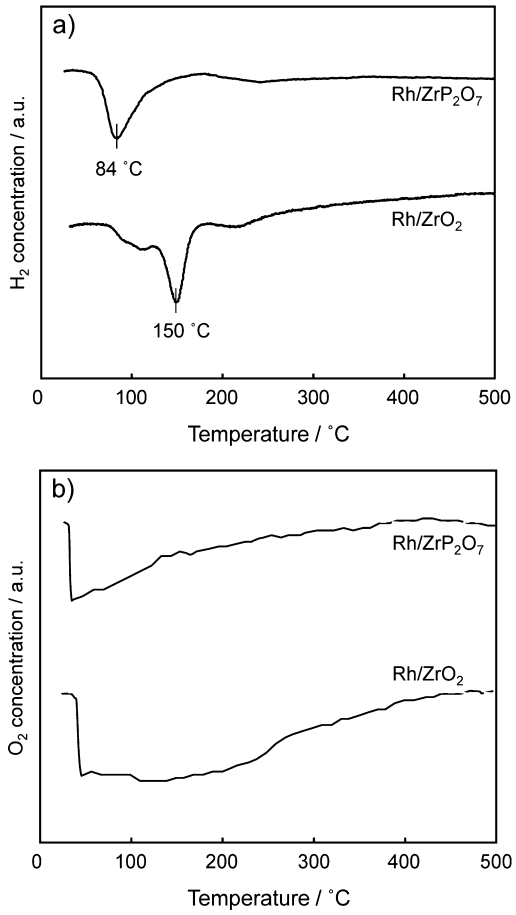

Figure 12. (a) H_2-TPR and (b) O_2-TPO profiles of as-prepared Rh/ZrP_2O_7 and Rh/ZrO_2 catalysts measured at a heating rate of 10 °C min^{-1}.

temperature of 84 °C for Rh/ZrP_2O_7, compared to the 150 °C required for Rh/ZrO_2. After H_2-TPR measurement and subsequent cooling to ambient temperature, the catalysts were heated in an O_2/He flow to record the O_2-TPO profile. Rh/ZrO_2 exhibited O_2 consumption from ambient temperature to 400 °C as a result of the reoxidation of metallic Rh to oxide. The total amount of oxygen consumed during the process was approximately equivalent to the stoichiometric reaction $2Rh + 1.5O_2 = Rh_2O_3$. Oxygen consumption in the case of Rh/ZrP_2O_7 was far below that observed for Rh/ZrO_2, suggesting a very slow reoxidation rate. Summarizing the results of the XANES, XPS, and TPR/TPO experiments, the ZrP_2O_7 support enables a higher reducibility of Rh oxide to metallic Rh, which is highly stable against reoxidation.

A similar unusual redox behavior was already observed for Rh/$AlPO_4$ in our previous report, which is associated with an Rh−O−P interfacial linkage via surface phosphate units.[11,12] This interaction is preserved under oxidizing and reducing atmospheres. The Rh oxide anchored by this interfacial linkage is easily reduced to active metallic Rh, whereas Rh−O−Al bonding formed in Rh/Al_2O_3 is very difficult to reduce. On the other hand, an electron-drawing effect from the phosphate group decreases the electron density of Rh metal and thus stabilizes against reoxidation to Rh oxide, compared with Rh

DOI: 10.1021/cs5020157
ACS Catal. 2015, 5, 1986−1994

metal on Al_2O_3. The formation of Rh−O−P bonding in the present Rh/ZrP_2O_7 catalyst was confirmed by Rh K-edge EXAFS (Supporting Information). It is therefore considered that the unusual redox behavior is a common feature of Rh catalysts supported on metal phosphate supports.

Possible Reason for the Higher deNO$_x$ Activity in Slightly Lean Regions. The present study demonstrates that Rh catalysts supported on metal phosphates exhibit a higher deNO$_x$ activity in slightly lean regions, which can be associated with the following two important features of the metal phosphate supports compared with metal oxide supports. First, the adsorption species of partially oxidized C_3H_6 are different. The oxidative adsorption of C_3H_6 onto Rh/ZrP_2O_7 forms aldehyde species whereas carboxylate species are formed on Rh/ZrO_2. Carboxylate is well-known as the surface species that is adsorbed on Pt/Al_2O_3,[24−26] Pt/ZSM-5,[27] and Au/TiO_2[28] in the reaction involving C_3H_6 and O_2. The carboxylate species on these catalysts are stable and monopolize the surface to inhibit the adsorption of O_2 and other reactants. As shown in Figures 8 and 9, the adsorbed carboxylate species formed on Rh/ZrO_2 show negligible changes upon admission of O_2 or NO. By contrast, the aldehyde species on Rh/ZrP_2O_7 are considered to be useful intermediates because of their higher reactivity toward O_2 and NO. Since aldehyde intermediates are formed on Rh/ZrP_2O_7, even under lean conditions, these species are considered to play a key role as reducing agents in the lean deNO$_x$ process.

The selective catalytic reduction of NO$_x$ by hydrocarbons (HC-SCR) under lean-burn conditions has been extensively studied in 1990s.[29−31] It is known that platinum group metals catalyze HC-SCR only when the reaction temperature is typically below 300 °C.[29,30,32,33] Although A/F for such HC-SCR reactions is much higher (A/F > 17.5), compared with the present slightly lean condition (A/F < 15.3), these previous studies give us valuable mechanistic information. For the most active Pt catalysts, various mechanistic studies have proposed two possible roles of hydrocarbon reductants (mostly C_3H_6) on the catalyst surface: (i) the reductants remove adsorbed oxygen and thus to enable NO dissociation to give N and O and subsequent desorption of N_2 and/or N_2O; (ii) the reductants form activated intermediate species that react with adsorbed NO. Although Nikolopoulos et al.[16] proposed the latter mechanism (ii) for Rh/Al_2O_3 based on their kinetic analysis, the intermediate species have not been identified so far. At this moment, it is not clear which mechanism prevails in the present Rh/ZrP_2O_7 catalyst. However, because the highly reactive aldehyde intermediate stored on the phosphate surface is able to react with O_2 as well as NO adsorbed on Rh (Figures 8 and 9), it should be effective for both cases.

As evident from Figure 7, the formation of the aldehyde species is highly dependent on the nature of phosphates. Unlike ZrP_2O_7 and $AlPO_4$, the formation of adsorbed aldehydes was less abundant in the case of YPO_4 and $LaPO_4$, which rather formed carboxylate species. Considering the following sequence of increasing ratio of aldehyde to carboxylate, ZrP_2O_7 > $AlPO_4$ > YPO_4 > $LaPO_4$, the acid−base properties of these metal phosphates seem to be an important factor determining the partially oxidized species. Here, the acid−base properties of the support materials are estimated using electronegativity, as proposed by Sanderson.[34−37] For a compound $X_xY_yZ_z$, the mean electronegativity (S) is the geometric mean of the electronegativities of each of the constituent atoms (S_X, S_Y, and S_Z) given by eq 1:

$$S = [S_X{}^x \cdot S_Y{}^y \cdot S_Z{}^z]^{1/(x+y+z)} \quad (1)$$

The obtained parameter has been successfully correlated with physicochemical properties such as the acidity of zeolites and the vibration spectra of metal phosphates.[35−37] Figure 13 shows

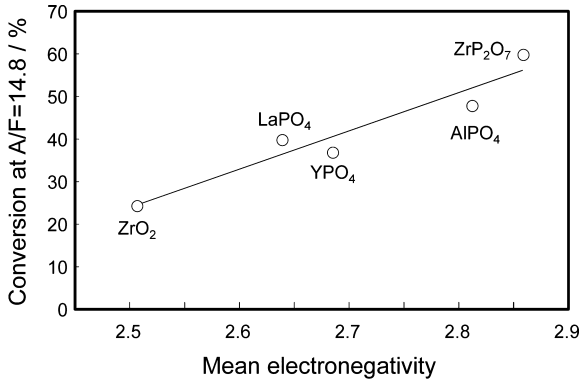

Figure 13. Relation between mean electronegativity of the support materials and lean NO$_x$ conversion at A/F = 14.8 (400 °C, mode A).

the relation between mean electronegativity of the present support materials and NO$_x$ conversion at A/F = 14.8 and 400 °C (mode A). Clearly, the NO$_x$ conversion efficiency tends to increase with an increase in the mean electronegativity, suggesting that the acid character of Rh/ZrP_2O_7 would be suitable for lean deNO$_x$ activity under the present slightly lean conditions.

Second, note that the catalytic activity of Rh is influenced by the oxidation state. Oxidized Rh (Rh^{3+}) is less active than metallic Rh in many reaction systems such as NO−C_3H_6, CO−O_2, and CH_4−O_2.[8,38−41] Haneda et al.[8] reported that Rh oxide (Rh_2O_3) formed on CeO_2−ZrO_2 is less active than metallic Rh for NO$_x$ reduction by hydrocarbons. Several studies have shown that the solid reaction between Rh oxide and Al_2O_3 in automotive TWCs in an oxidizing atmosphere results in serious deactivation,[42−47] because it is difficult to reduce the obtained Rh oxide back to the metallic state. These reports suggest that strong interactions between Rh oxide and the oxide supports are the main cause for the lack of reducibility. Note that the Rh oxide formed on ZrP_2O_7 in the present study does not follow this trend; its reduction is much easier than that of the Rh oxide formed on the corresponding oxide support, ZrO_2 (Figure 12). Also, metallic Rh is further stabilized against oxidation in the presence of excess O_2 on ZrP_2O_7 (Figures 10 and 11). A higher fraction of metallic Rh in Rh/ZrP_2O_7 favors adsorption and activation of NO, whereas a higher fraction of the aldehyde species on the ZrP_2O_7 surface further favors the reaction between surface oxygen via spillover effect and aldehyde species. Consequently, the high activity of Rh/ZrP_2O_7 for C_3H_6 oxidation via aldehyde species as well as metallic Rh showing tolerance against reoxidation on this support are considered to be possible reasons for the enhanced deNO$_x$ performance of Rh/ZrP_2O_7 in a slightly lean region, although further examinations may be required to obtain a conclusive reaction mechanism.

CONCLUSION

The present study has demonstrated that ZrP_2O_7 is an interesting support material for Rh catalysts enabling a high NO$_x$ purification performance in a slightly lean region (14.6 <

DOI: 10.1021/cs5020157
ACS Catal. 2015, 5, 1986−1994

$A/F \leq 15.3$). Among the four studied Rh catalysts supported on different metal phosphates ($AlPO_4$, ZrP_2O_7, YPO_4, and $LaPO_4$), Rh/ZrP_2O_7 exhibits the highest NO_x conversion efficiency at $A/F = 14.8$. The conversion is two times larger than that determined for Rh/ZrO_2 and is considered to be the result of preferential $NO-C_3H_6$ and NO−CO reactions in the presence of excess O_2. A larger contribution of the $NO-C_3H_6$ reaction is associated with oxidatively adsorbed C_3H_6 in the form of aldehyde species having a higher reactivity to O_2 and NO on Rh/ZrP_2O_7 compared with the less-active carboxylate species on Rh/ZrO_2. The higher activity under lean conditions is also associated with the unusual redox behavior of Rh. The reduction of Rh oxide to metallic Rh is easier on ZrP_2O_7 than on ZrO_2. Moreover, the metallic Rh species formed on ZrP_2O_7 are stable against reoxidation, whereas those formed on ZrO_2 are immediately reoxidized to Rh oxide in excess O_2.

■ ASSOCIATED CONTENT

Supporting Information

The following file is available free of charge on the ACS Publications website at DOI: 10.1021/cs5020157.

XRD of metal phosphates, *in situ* FT-IR of C_3H_6 and pyridine adsorbed, Rh K-edge EXAFS of supported Rh catalysts, and composition of simulated exhaust gas mixtures for catalytic tests (PDF)

■ AUTHOR INFORMATION

Corresponding Authors

*E-mail: machida@kumamoto-u.ac.jp. Fax: 096-342-3651.
*E-mail: y_nagao@mitsui-kinzoku.co.jp. Fax: 048-775-8153.

Notes

The authors declare no competing financial interest.

■ ACKNOWLEDGMENTS

This study was supported by the "Elements Science and Technology Project" of the Ministry of Education, Culture, Sports, Science, and Technology (MEXT) Japan and the MEXT program "Elements Strategy Initiative to Form Core Research Centers." XAFS experiments were performed at the BL14B2 beamline of SPring-8 with the approval of the Japan Synchrotron Radiation Research Institute (JASRI) (Proposal No. 2013A1344).

■ REFERENCES

(1) Heck, R. M.; Farrauto, R. J.; Gulati, S. T. *Catalytic Air Pollution Control: Commercial Technology*; Wiley: Hoboken, NJ, 1995.
(2) Shelef, M. *Catal. Rev. Sci. Eng.* **1975**, *11*, 1−40.
(3) Taylor, K. C. *Catal. Rev. Sci. Eng.* **1993**, *35*, 457−481.
(4) Farrauto, R. J.; Heck, R. M. *Catal. Today* **1999**, *51*, 351−360.
(5) Shelef, M.; McCabe, R. W. *Catal. Today* **2000**, *62*, 35−50.
(6) Gandhi, H. S.; Graham, G. W.; McCabe, R. W. *J. Catal.* **2003**, *216*, 433.
(7) Shelef, M.; Graham, G. W. *Catal. Rev. Sci. Eng.* **1994**, *36*, 433−457.
(8) Haneda, M.; Houshito, O.; Takagi, H.; Shinoda, K.; Nakahara, Y.; Hiroe, K.; Fujitani, T.; Hamada, H. *Top. Catal.* **2009**, *52*, 1868−1872.
(9) Machida, M.; Murakami, K.; Hinokuma, S.; Uemura, K.; Ikeue, K.; Matsuda, M.; Chai, M. R.; Nakahara, Y.; Sato, T. *Chem. Mater.* **2009**, *21*, 1796−1798.
(10) Ikeue, K.; Murakami, K.; Hinokuma, S.; Uemura, K.; Zhang, D. J.; Machida, M. *Bull. Chem. Soc. Jpn.* **2010**, *83*, 291−297.
(11) Machida, M.; Minami, S.; Ikeue, K.; Hinokuma, S.; Nagao, Y.; Sato, T.; Nakahara, Y. *Chem. Mater.* **2014**, *26*, 5799−5805.
(12) Machida, M.; Minami, S.; Yoshida, H.; Hinokuma, S.; Nagao, Y.; Sato, T.; Nakahara, Y. *J. Phys. Chem. C* **2015**, *119*, 373−380.
(13) Takeguchi, T.; Manabe, S.; Kikuchi, R.; Eguchi, K.; Kanazawa, T.; Matsumoto, S.; Ueda, W. *Appl. Catal. A: Gen.* **2005**, *293*, 91−96.
(14) Ravel, B.; Newville, M. *J. Synchrotron Radiat.* **2005**, *12*, 537−541.
(15) Tanaka, H.; Hirotoshi, F.; Takahashi, I. *SAE Paper* **1995**, Paper No. 950256.
(16) Nikolopoulos, A. A.; Stergioula, E. S.; Efthimiadis, E. A.; Vasalos, I. A. *Catal. Today* **1999**, *54*, 439−450.
(17) Halkides, T. I.; Kondarides, D. I.; Verykios, X. E. *Catal. Today* **2002**, *73*, 213−221.
(18) Chauvin, C.; Saussey, J.; Lavalley, J.-C.; Idriss, H.; Hindermann, J.-P.; Kiennemann, A.; Chaumette, P.; Courty, P. *J. Catal.* **1990**, *121*, 56−69.
(19) Finocchio, E.; Daturi, M.; Binet, C.; Lavalley, J. C.; Blanchard, G. *Catal. Today* **1999**, *52*, 53−63.
(20) Bielansky, A.; Haber, J. *Oxygen in Catalysis*; Marcel Dekker: New York, 1991.
(21) K. Grasselli, R.; Centi, G.; Trifiro, F. *Appl. Catal.* **1990**, *57*, 149−166.
(22) Zhou, B.; Chuang, K. T.; Guo, X. *J. Chem. Soc., Faraday Trans.* **1991**, *87*, 3695−3702.
(23) Contour, J. P.; Mouvier, G.; Hoogewys, M.; Leclere, C. *J. Catal.* **1977**, *48*, 217−228.
(24) Wan, J.; Ran, R.; Li, M.; Wu, X.; Weng, D. *J. Mol. Catal. A: Chem.* **2014**, *383−384*, 194−202.
(25) Haneda, M.; Watanabe, T.; Kamiuchi, N.; Ozawa, M. *Appl. Catal. B: Environ.* **2013**, *142−143*, 8−14.
(26) Matsouka, V.; Konsolakis, M.; Lambert, R. M.; Yentekakis, I. V. *Appl. Catal. B: Environ.* **2008**, *84*, 715−722.
(27) Xin, M.; Hwang, I. C.; Woo, S. I. *Catal. Today* **1997**, *38*, 187−192.
(28) Ruiz, A.; van der Linden, B.; Makkee, M.; Mul, G. *J. Catal.* **2009**, *266*, 286−290.
(29) Burch, R.; Breen, J. P.; Meunier, F. C. *Appl. Catal. B: Environ.* **2002**, *39*, 283−303.
(30) Fritz, A.; Pitchon, V. *Appl. Catal. B: Environ.* **1997**, *13*, 1−25.
(31) Iwamoto, M.; Hamada, H. *Catal. Today* **1991**, *10*, 57−71.
(32) Obuchi, A.; Ohi, A.; Nakamura, M.; Ogata, A.; Mizuno, K.; Ohuchi, H. *Appl. Catal. B: Environ.* **1993**, *2*, 71−80.
(33) Hamada, H.; Kintaichi, Y.; Sasaki, M.; Ito, T.; Tabata, M. *Appl. Catal.* **1991**, *75*, L1−L8.
(34) Sanderson, R. T. *Chemical Bonds and Bond Energy*, 2nd ed.; Academic Press: New York, 1976.
(35) Hočevar, S.; Držaj, B. *J. Catal.* **1982**, *73*, 205−215.
(36) Mortier, W. J. *J. Catal.* **1978**, *55*, 138−145.
(37) Vaimakis, T. C.; Pomonis, P. J.; Sdoukos, A. T. *React. Kinet. Catal. Lett.* **1988**, *37*, 169−174.
(38) Dohmae, K.; Nagai, Y.; Tanabe, T.; Suzuki, A.; Inada, Y.; Nomura, M. *Surf. Interface Anal.* **2008**, *40*, 1751−1754.
(39) Grunwaldt, J.-D.; Basini, L.; Clausen, B. S. *J. Catal.* **2001**, *200*, 321−329.
(40) Zimowska, M.; Wagner, J. B.; Dziedzic, J.; Camra, J.; Borzęcka-Prokop, B.; Najbar, M. *Chem. Phys. Lett.* **2006**, *417*, 137−142.
(41) Shimizu, K.-i.; Oda, T.; Sakamoto, Y.; Kamiya, Y.; Yoshida, H.; Satsuma, A. *Appl. Catal. B: Environ.* **2012**, *111−112*, 509−514.
(42) Yao, H. C.; Japar, S.; Shelef, M. *J. Catal.* **1977**, *50*, 407−418.
(43) Yao, H. C.; Stepien, H. K.; Gandhi, H. S. *J. Catal.* **1980**, *61*, 547−550.
(44) Wong, C.; McCabe, R. W. *J. Catal.* **1989**, *119*, 47−64.
(45) Chen, J. G.; Colaianni, M. L.; Chen, P. J.; Yates, J. T., Jr; Fisher, G. B. *J. Phys. Chem.* **1990**, *94*, 5059−5062.
(46) McCabe, R. W.; Usmen, R. K.; Ober, K.; Gandhi, H. S. *J. Catal.* **1995**, *151*, 385−393.
(47) Beck, D. D.; Capehart, T. W.; Wong, C.; Belton, D. N. *J. Catal.* **1993**, *144*, 311−324.
(48) Gallaher, G.; Goodwin, J. G., Jr; Huang, C.-S.; Houalla, M. *J. Catal.* **1991**, *127*, 719−731.

DOI: 10.1021/cs5020157
ACS Catal. 2015, 5, 1986−1994